A Virtual Inertia Control Strategy for DC Microgrids Analogized with Virtual Synchronous Machines

Wu, Wenhua; Chen, Yandong; Luo, An; Zhou, Leming; Zhou, Xiaoping; Yang, Ling; Dong, Yanting; Guerrero, Josep M.

Published in:
I E E E Transactions on Industrial Electronics

DOI (link to publication from Publisher):
10.1109/TIE.2016.2645898

Publication date:
2017

Document Version
Early version, also known as pre-print

A Virtual Inertia Control Strategy for DC Microgrids Analogized with Virtual Synchronous Machines

Wenhua Wu, *Student Member, IEEE*, Yandong Chen, *Member, IEEE*, An Luo, *Senior Member, IEEE*, Leming Zhou, Xiaoping Zhou, *Student Member, IEEE*, Ling Yang, *Student Member, IEEE*, Yanting Dong, and Josep M. Guerrero, *Fellow, IEEE*

***Abstract*—In a DC microgrid (DC-MG), the dc bus voltage is vulnerable to power fluctuation derived from the intermittent distributed energy or local loads variation. In this paper, a virtual inertia control strategy for DC-MG through bidirectional grid-connected converters (BGCs) analogized with virtual synchronous machine (VSM) is proposed to enhance the inertia of the DC-MG, and to restrain the dc bus voltage fluctuation. The small-signal model of the BGC system is established, and the small-signal transfer function between the dc bus voltage and the dc output current of the BGC is deduced. The dynamic characteristic of the dc bus voltage with power fluctuation in the DC-MG is analyzed in detail. As a result, the dc output current of the BGC is equivalent to a disturbance, which affects the dynamic response of the dc bus voltage. For this reason, a dc output current feed-forward disturbance suppressing method for the BGC is introduced to smooth the dynamic response of the dc bus voltage. By analyzing the control system stability, the appropriate virtual inertia control parameters are selected. Finally, simulations and experiments verified the validity of the proposed control strategy.**

***Index Terms*—DC microgrid, bidirectional grid-connected converter, power fluctuation, virtual inertia control, small-signal modeling, disturbance suppressing.**

I. INTRODUCTION

DC microgrids (DC-MGs) have been developed rapidly due to the penetration of distributed generations (DGs), energy storage, and the local dc loads [1]-[3]. As the interface between the DC-MG and the utility grid, bidirectional grid-connected converters (BGCs) play a significant role in controlling the energy exchange between the DC-MG and the utility grid, maintaining the dc bus voltage stability, and improving the system efficiency [4], [5]. However, the DC-MG is a low-inertia grid dominated by power electronic converters. The frequent switching loads and intermittent DGs (e.g. PV source, wind resource) can give rise to large volatility of the dc bus voltage [6], and reduce the efficiency and stability of the DC-MG [7]. Introducing the virtual inertia control into the BGC is a promising way to increase the inertia of DC-MG, to diminish fluctuation of the dc bus voltage, and to enhance the stability of the DC-MG.

Currently, researches about the virtual inertia control of power electronic converters mainly focus on the active support to the utility grid or the AC microgrid (AC-MG). A common virtual inertia control strategy is to operate converters as virtual synchronous machines (VSMs) [8]-[19]. The rotor inertia of the synchronous machine (SM) is emulated by combining the energy storage with the converters in [8]. The concept of the synchronverter is firstly proposed in [9], [10], which is similar to the SM in mechanical and electrical characteristics by establishing the electromagnetic and mechanical equations of the SM. Due to its superior control performance, the VSM control is successfully applied to modular multilevel converters (MMCs) [11], doubly fed induction generator (DFIG)-based wind turbines [12], voltage source converter (VSC) stations [13], and energy storage systems [14]. In order to suppress power fluctuation of the VSM, J. Alipoor et al. [15] propose the bang-bang control method used on virtual rotor inertia of the VSM by adaptively changing its inertia parameters. In [16], [17], an oscillation damping method is proposed to avoid the low-frequency oscillation of the VSM. In [18], a small-signal model of the VSM is built, and its control parameters design method is also provided by analyzing the system stability and dynamic performance. In [19], the comparisons of the dynamic characteristics between the VSM control and droop control are analyzed in detail, and prove that the VSM control owns more advantages.

However, researches on the virtual inertia control for DC-MG are hardly reported. The DC-MG often adopts power- or

Manuscript received June 30, 2016; revised September 30, 2016; accepted November 20, 2016. This work was supported in part by the National Natural Science Foundation of China under Grant 51577056 and in part by Scientific Research Fund of Hunan Provincial Education Department under Grant YB2016B036.

W. Wu, A. Luo, L. Zhou, X. Zhou, L. Yang, and Y. Dong are with the College of Electrical and Information Engineering, Hunan University, Changsha 410082, China (e-mail: wenhua_5@163.com; an_luo@126.com; leming_zhou@126.com; zxp2011@hnu.edu.cn; yangling_1992@163.com; KarenDongyt@163.com).

J. M. Guerrero is with the Department of Energy Technology, Aalborg University, 9220 Aalborg East, Denmark (e-mail: joz@et.aau.dk).

Y. Chen are with the College of Electrical and Information Engineering, Hunan University, Changsha 410082, China (corresponding author, phone: +86-731-88823710; fax: +86-731-88823700; e-mail: yanong_chen@hnu.edu.cn).

current-based droop controller to stabilize the dc bus voltage [20]. However, there exists a trade-off between the voltage deviation and current sharing accuracy. By the low bandwidth communication, the improved droop control method can restore the dc bus voltage and enhance the current sharing accuracy [21]. DC bus signaling (DBS) is presented as a prominent decentralized coordination method for DC-MG [22]. Using the DBS approach, the different operating modes of the converters can be coordinated according to the magnitude of dc bus voltage to maintain the dc bus voltage. In [23], a soft-start voltage control strategy is proposed to improve the transient response during the initial startup of power converters. In [24], a ripple elimination method is proposed to restrain the dc bus voltage ripples. The tradeoff between the current distortion and bandwidth of dc bus voltage control of the converter is analyzed and solved in [25]. In large scale dc distribution systems with high penetration of DG units, a multi-agent distributed voltage regulation scheme is proposed to mitigate the voltage regulation challenges [26]. However, the above dc voltage regulation methods are not to discuss how to enhance the inertia of DC-MG. To this issue, an approach using super-capacitors to suppress the dc bus voltage fluctuation is presented to improve the inertia of DC-MG when the local loads or DGs suddenly change [27]. But the costs of super-capacitors are relatively high. Moreover, when the DC-MG is in the steady-state operation, these super-capacitors are idle, which causes resource waste. In [28], a virtual inertia control strategy of the wind-battery-based islanded DC-MG is presented. By adding a high-pass filter into the additional inertia control loop, these converters can keep the power balance of the DC-MG when the dc bus voltage suddenly changes. But the high-pass filter may bring in the high-frequency disturbance.

In this paper, the idea of migrating the relatively mature VSM control strategy into the BGC for improving the inertia of the DC-MG is studied. The remainder of this paper is organized as follows: the structure of the inertia-enhanced DC-MG with a BGC is introduced, and a virtual inertia control strategy for the BGC analogized with VSMs is proposed in Section II, Then, the small-signal model of the BGC system is built in Section III. In Section IV, the dynamic performance of the BGC system is analyzed, and the dc output current feedforward disturbance suppressing method for the BGC is introduced to further improve the dynamic response of the dc bus voltage. The BGC control system stability analysis and parameters selection are discussed in Section V. Simulations and experiments verify the theoretical analysis in Section VI. Finally, some conclusions are given in Section VII.

II. VIRTUAL INERTIA CONTROL STRATEGY OF THE BGC

A. DC-MG structure with a BGC

As shown in Fig. 1, the inertia-enhanced DC-MG consists of a BGC, DGs, energy storages, loads and relevant power electronic converters. The main circuit of the BGC adopts the three-phase full-bridge converter, where C is the dc-link output capacitor, L is the input filter inductor, r is the equivalent series resistance of the L, u_j (j=a, b, c) is the utility grid voltage, i_j is the grid-connected current, e_j is the voltage of the BGC on the ac side, u_{dc} is the dc bus voltage of the DC-MG, i_{dc} is the dc-link current of the full-bridge converter, and i_o is the dc output current of the BGC.

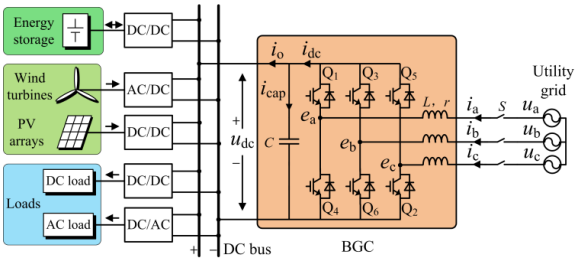

Fig. 1. An inertia-enhanced DC-MG structure with a BGC.

When the DC-MG is operating in grid-connected mode, the BGC is responsible for keeping the power balance of the DC-MG through the bidirectional energy exchange with the utility grid, which ensures the stability of the dc bus voltage. The maximum power point tracking control is used in the DGs. The energy storage units are charged with the rated current when they are not completely charged. Loads connected to the dc bus are mainly constant power loads. In this mode, the DGs, energy storage units and loads can be regarded as current sources connected to the dc bus, and the dc bus voltage is regulated by the BGC. When the DC-MG is in the islanded mode, the BGC is out of service.

B. Inertia analogy between AC-MG and DC-MG

In an AC-MG, the active power-frequency (P-ω) control of the VSM emulates inertia, damping characteristic and the primary frequency regulation of the SM. In this paper, it is assumed that the number of pairs of poles for the VSM is 1, thus the mechanical equation [16] can be described as

$$P_{set} - P_e - D_p(\omega - \omega_n) = J\omega\frac{d\omega}{dt} \approx J\omega_n\frac{d\omega}{dt} \tag{1}$$

where P_{set}, P_e, D_p, ω, ω_n are the active power reference, the electromagnetic power, the damping coefficient, the angular frequency of the VSM, and the rated angular frequency of the utility grid, respectively. J is the virtual moment of inertia.

When the AC-MG is in steady state, (1) can be rewritten as

$$\omega = \omega_{no} - mP_e \tag{2}$$

where $\omega_{no} = \omega_n + P_{set}/D_p$ is the no-load angular frequency, and $m = 1/D_p$ is the droop coefficient. It can be known from (1) and (2) that the P-ω control of VSM is actually a modified droop control.

In the DC-MG, the voltage-current droop control is usually adopted for the BGC. There are three advantages as follows:

1) System stability of the DC-MG with constant power loads can be improved [29], [30].

2) It is easy to expand the system capacity by paralleling BGCs [31].

3) Coordinated control based on the bus-signaling for the DC-MG is easy to be realized [32].

The voltage-current droop control of the BGC can be expressed as

$$u_{dc}^* = U_{dc\_ref} - R_v i_o \tag{3}$$

where U_{dc_ref} is the no-load dc output voltage reference of the BGC, R_v is the droop coefficient, and u_{dc}^* is the reference value of the dc bus voltage of the DC-MG.

For the AC-MG, inertia of the system manifests the ability to prevent sudden changes of the frequency, and thereby leaving SM enough time to regulate the active power P_e, then rebuilding balance of the active power. For the DC-MG, its inertia manifests the ability to prevent sudden changes of the dc bus voltage u_{dc}. BGC can quickly extract or inject the current i_o from or to the DC-MG, maintaining the voltage stability of the DC-MG. Comparing with the droop expressions (2) and (3), it can be shown that ω and u_{dc}, P_e and i_o are comparable in form. It is also mentioned in [33] that the current sharing (the voltage-current droop control) of the DC-MG is similar to the active power sharing in the resistive-line AC-MG.

The kinetic energy W_r saved in the rotor of the SM, and the electric energy W_c saved in the capacitors connected to the dc bus in DC-MG are defined as:

$$\begin{cases} W_r = \frac{1}{2} J\omega^2 \\ W_c = \frac{1}{2} C u_{dc}^{\ 2} \end{cases} \tag{4}$$

When the frequency of an AC-MG suffers from disturbance, the rotor can quickly provide active power support. Similarly, when the dc bus voltage of a DC-MG suffers from disturbance, the capacitors can quickly provide active power support.

From the above analysis, it is obvious that many variables and characteristics are mutually corresponding between the AC-MG containing a VSM and the DC-MG containing a BGC, as shown in Table I.

TABLE I
ANALOGY BETWEEN AC-MG AND DC-MG

Microgrids	AC-MG containing a VSM	DC-MG containing a BGC
Droop relation	ω-P_e droop	u_{dc}-i_o droop
Control target	ω	u_{dc}
Output	P_e	i_o
Inertia	J	C
Stored energy	$0.5J\omega^2$	$0.5Cu_{dc}^2$

C. The virtual inertia control strategy for DC-MGs

As shown in Fig. 2, the virtual inertia control equation of the BGC similar to (1) is proposed via analogizing with the VSM, where I_{set} is the dc output current reference of the BGC, D_b is the droop coefficient, U_n is the rated dc bus voltage, and C_v is the introduced virtual capacitance. Obviously, it is reasonable to enhance the inertia of the DC-MG by introducing the virtual inertia control into the BGC.

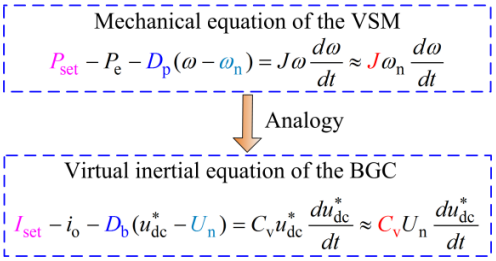

Fig. 2. Virtual inertia equation of the BGC via analogizing with the VSM.

Fig. 3 shows the block diagram of the virtual inertia control strategy for DC-MGs analogized with virtual synchronous machines, which mainly includes the virtual inertia control, dc output current feed-forward control, and voltage and current dual-loop control.

In terms of the virtual inertia equation of the BGC, the virtual inertia control is presented to enhance the inertia of the DC-MG, and to restrain the dc bus voltage fluctuation. The output of the virtual inertia control is regarded as the dc bus voltage reference u_{dc}^*.

The dc output current feed-forward control is introduced to improve the dynamic performance of the dc bus voltage, and to suppress the disturbance derived from the dc output current of the BGC. $G_{ff}(s)$ is the transfer function of the dc output current feed-forward control.

The voltage and current dual-loop control consists of the PI voltage outer loop control to track accurately the dc bus voltage reference, and the current inner loop control based on synchronous reference frames (SRFs) to realize active power exchange with the utility grid. u_d and u_q are the d-axis and q-axis components of u_j in the SRFs, respectively. i_d and i_q are the d-axis and q-axis components of i_j in the SRFs, respectively. i_d^* and i_q^* are the current reference of i_d and i_q, respectively.

III. SMALL-SIGNAL MODELING OF THE BGC SYSTEM

In order to find out the relation between the dc bus voltage and power demand of the DC-MG, it is necessary to build the BGC small-signal model. From Fig. 1, the mathematical expression of the BGC in the SRFs is described as

$$\begin{cases} u_d = (Lp + r)i_d - \omega_g L i_q + e_d \\ u_q = (Lp + r)i_q + \omega_g L i_d + e_q \end{cases} \tag{5}$$

where p is the differential operator, and ω_g is the angular frequency of the utility grid voltage. e_d and e_q are the d-axis and q-axis components of e_j in the SRFs, respectively.

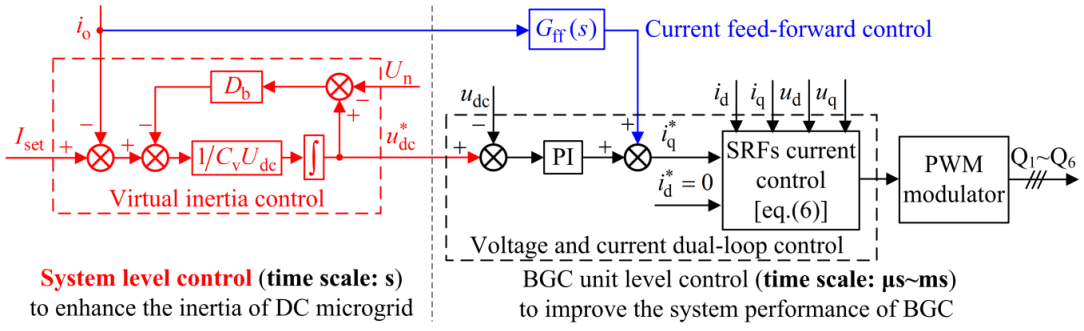

Fig. 3. Block diagram of the virtual inertia control strategy for DC-MGs analogized with virtual synchronous machines

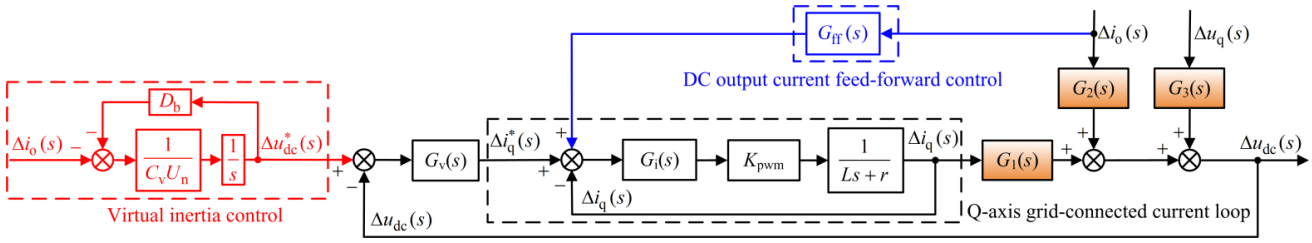

Fig. 4. The small-signal model of the BGC control system.

From (5), it is clear that the BGC variables in the d-axis and q-axis are mutually coupling, which makes it difficult to design the controller. Here, the SRFs current control is adopted. PI controller is used for the grid-connected current control, which is represented as $G_i(s) = k_{pi} + k_{ii}/s$, thus the inner current control equation can be expressed as

$$\begin{cases} e_d = -G_i(s)(i_d^* - i_d) + \omega_g L i_q + u_d \\ e_q = -G_i(s)(i_q^* - i_q) - \omega_g L i_d + u_q \end{cases}. \tag{6}$$

Substituting e_d and e_q from (6) to (5), the following expression can be obtained:

$$\begin{cases} (Lp + r) i_d = (i_d^* - i_d) G_i(s) \\ (Lp + r) i_q = (i_q^* - i_q) G_i(s) \end{cases}. \tag{7}$$

Assume that the state variables in (7) are written as the sum of steady-state variables and their small perturbations ($i_d = I_d + \Delta i_d$ and $i_q = I_q + \Delta i_q$). Ignoring the second-order perturbations, and applying the Laplace transform, the corresponding small-signal equation can be expressed as follows

$$\begin{cases} \Delta i_d(s) = [\Delta i_d^*(s) - \Delta i_d(s)] G_i(s) / (Ls + r) \\ \Delta i_q(s) = [\Delta i_q^*(s) - \Delta i_q(s)] G_i(s) / (Ls + r) \end{cases}. \tag{8}$$

Considering symmetry of the grid-connected current inner loops in d-axis and q-axis, the q-axis is taken as an example in order to simplify the analysis. Ignoring the influence of the current sampling delay, PWM control delay, and the perturbation component Δu_q, the small-signal model of the q-axis grid-connected current inner loop is obtained based on (8), as shown in Fig. 4, where K_{pwm} is the equivalent gain of pulse width modulator.

Then the control structure of the dc bus voltage outer loop is built. And the small-signal model of the BGC system can be deducted. Neglecting the energy loss, according to the power balance between two sides of the BGC, there is:

$$1.5(u_d i_d + u_q i_q) = u_{dc} i_{dc} = u_{dc}(C \frac{du_{dc}}{dt} + i_o). \tag{9}$$

The state variables in (9) are written as the sum of steady state variables and small perturbations ($u_d = U_d + \Delta u_d$, $u_q = U_q + \Delta u_q$, $u_{dc} = U_{dc} + \Delta u_{dc}$, $i_o = I_o + \Delta i_o$). If the second-order perturbations are ignored, the small-signal equation of (9) can be described as

$$1.5(U_d \Delta i_d + U_q \Delta i_q + \Delta u_d I_d + \Delta u_q I_q) = C U_{dc} \frac{d\Delta u_{dc}}{dt} + U_{dc} \Delta i_o + \Delta u_{dc} I_o. \tag{10}$$

When the grid-voltage-oriented control is used in the BGC, U_d is equivalent to zero in steady state. BGC is only used to control the dc bus voltage, and does not provide reactive power to the utility grid, so the reactive current component I_d is zero. Thus, the expression (10) can be simplified as

$$1.5(U_q \Delta i_q + \Delta u_q I_q) = C U_{dc} \frac{d\Delta u_{dc}}{dt} + U_{dc} \Delta i_o + \Delta u_{dc} I_o. \tag{11}$$

According to the superposition theorem, ignoring the perturbation components Δu_q and Δi_o, and applying the Laplace transformation to (11), the relation between $u_{dc}(s)$ and $i_q(s)$ is obtained as follows:

$$\Delta u_{dc}(s) / \Delta i_q(s) = 3U_q / 2(CU_{dc} s + I_o) = G_1(s). \tag{12}$$

Similarly, the relations between $\Delta u_{dc}(s)$ and $\Delta i_o(s)$, $\Delta u_{dc}(s)$ and $\Delta u_q(s)$ are respectively obtained as the follows

$$\Delta u_{dc}(s) / \Delta i_o(s) = -U_{dc} / (CU_{dc} s + I_o) = G_2(s), \tag{13}$$

$$\Delta u_{dc}(s) / \Delta u_q(s) = 3I_q / 2(CU_{dc} s + I_o) = G_3(s). \tag{14}$$

Performing the small-signal decomposition, the virtual inertia equation of the BGC in Fig. 2 can be expressed as

$$-\Delta i_o - D_b \Delta u_{dc}^* = C_v U_n \frac{d\Delta u_{dc}^*}{dt} \tag{15}$$

where Δu_{dc}^* is the small-signal perturbation of u_{dc}^*. Then applying the Laplace transform, (15) can be rewritten as

$$\Delta u_{dc}^*(s) = (-\Delta i_o(s) - D_b \Delta u_{dc}^*(s)) / s C_v U_n. \tag{16}$$

According to (12)-(14), (16) and Fig. 3, the small-signal model of the BGC control system can be derived as shown in Fig. 4, where $G_v(s)$ is the transfer function of dc bus voltage regulator using the PI regulator ($G_v(s) = k_{pv} + k_{iv}/s$).

IV. DYNAMIC PERFORMANCE ANALYSIS AND THE DC OUTPUT CURRENT FEED-FORWARD CONTROL

In Fig. 4, ignoring the influence of the utility grid voltage, and if the dc output current feed-forward control is not adopted, the small-signal closed-loop transfer function $TF(s)$ between $\Delta u_{dc}(s)$ and $\Delta i_o(s)$ is obtained as follows:

$$TF(s) = \frac{\Delta u_{dc}(s)}{\Delta i_o(s)} = \frac{G_{vir}(s) G_v(s) G_c(s) G_1(s) + G_2(s)}{1 + G_v(s) G_c(s) G_1(s)} \tag{17}$$

where $G_{vir}(s) = -1/(D_b + C_v U_n s)$, $G_c(s) = G_i(s) K_{pwm} / (G_i(s) K_{pwm} + Ls + r)$.

Fig. 5 shows the unit-step responses of $TF(s)$ for various values of C_v when D_b is 5 or 1. The physical meaning of the unit-step response is the dc bus voltage change when the BGC output current suddenly increases. As is known to all, the dc output current of the BGC is relevant to the power demand of the DC-MG which is decided by the power consumption of the loads and the output power of DG sources. In Fig. 5(a), the

red solid points represent the positions where the step response curve reaches the 95% of the steady state value.

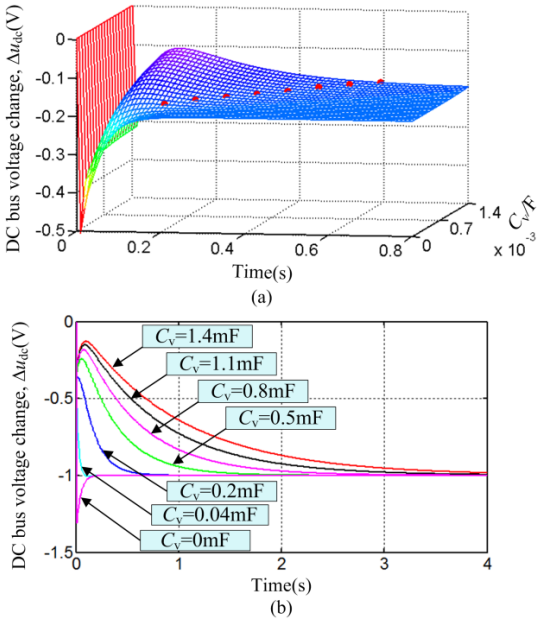

Fig. 5. Unit-step responses of $TF(s)$ for various values of C_v. (a) D_b = 5. (b) D_b = 1.

It can be seen from Fig. 5 that the dc bus voltage would change more mildly when C_v increases if the initial stage of the step response is neglected, which indicates that the inertia of the DC-MG is larger. When C_v is less than 0.04mF, the dc bus voltage changes quickly, and the inertia of the DC-MG is very small. As a result, the value of C_v directly determines the inertia of the DC-MG.

From Fig. 5, it is clear that the dc bus voltage at the initial stage of all step response with different D_b and C_v has a serious impact. The abrupt voltage changes at the beginning of the unit-step response process would do harm to the realization of virtual inertia of the DC-MG, jeopardizing the dynamic performance of the dc bus voltage.

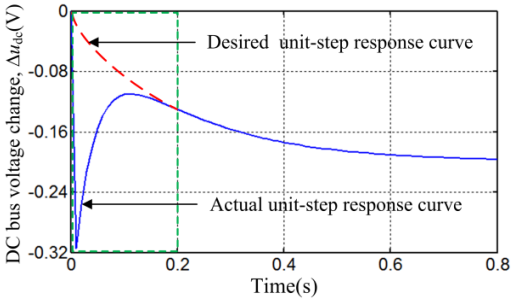

Fig. 6. Unit-step responses of $TF(s)$ when D_b = 5, C_v = 1.4mF.

To further analyze the impact mentioned above, the unit-step response of $TF(s)$ when D_b = 5, C_v = 1.4mF is shown in Fig. 6. At the initial stage of unit-step response, the dc bus voltage occurs to the sudden drop and up phenomenon. Thus, to further improve the dynamic performance of the dc bus voltage, the actual unit-step response would be amended to the desired unit-step response shown in Fig. 6.

As shown in Fig. 4, $\Delta i_o(s)$ can affect $\Delta u_{dc}(s)$ through two loops (loop1 and loop2). Loop1: $\Delta i_o(s)$ affects $\Delta u_{dc}(s)$ through $G_2(s)$ and voltage and current dual-loop control. Loop2: $\Delta i_o(s)$ affects $\Delta u_{dc}(s)$ through the virtual inertia control and the voltage and current dual-loop control. Ignoring the influence of the ESR of the filter inductor, the transfer functions of the two loops $TF_{loop1}(s)$ and $TF_{loop2}(s)$ are derived as:

$$TF_{loop1}(s)=\frac{(G_i(s)K_{pwm}+Ls)G_2(s)}{G_i(s)K_{pwm}G_v(s)G_l(s)+G_i(s)K_{pwm}+Ls}. \quad (18)$$

$$TF_{loop2}(s)=\frac{-G_i(s)K_{pwm}G_v(s)G_l(s)/(D_b+C_vU_ns)}{G_i(s)K_{pwm}G_v(s)G_l(s)+G_i(s)K_{pwm}+Ls}. \quad (19)$$

Clearly, the transfer function $TF(s)$ of $\Delta u_{dc}(s)$ and $\Delta i_o(s)$ can be split into two parts:

$$TF(s)=TF_{loop1}(s)+TF_{loop2}(s). \quad (20)$$

Fig. 7 illustrates the unit-step responses of $TF_{loop1}(s)$ and $TF_{loop2}(s)$. A notch appears at the begining of the unit-step response of $TF_{loop1}(s)$. Over time, this response would finally reach zero. However, the unit-step response of the $TF_{loop2}(s)$ would smoothly decline to the steady state value. So, the serious impact at the initial stage is caused by $TF_{loop1}(s)$, thus $\Delta i_o(s)$ passing through loop1 is equivalent to perturbation, which affects the smoothness of the dc bus voltage dynamic response.

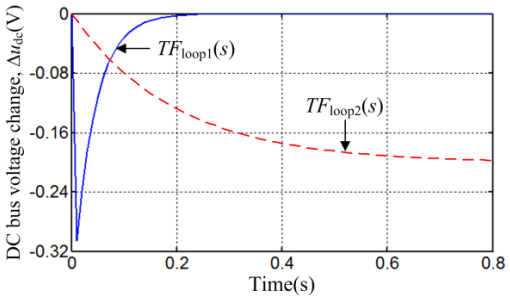

Fig. 7. Unit-step responses of $TF_{loop1}(s)$ and $TF_{loop2}(s)$.

Here, dc output current feed-forward control for the BGC is introduced to eliminate the serious impact from the disturbing loop1, which can improve the dynamic performance of the dc bus voltage. The transfer function $G_{ff}(s)$ of dc output current feed-forward control in Fig. 4 is expressed as follows:

$$G_{ff}(s)=\frac{-G_2(s)(K_{pwm}G_i(s)+Ls+r)}{K_{pwm}G_i(s)G_l(s)} \quad (21)$$

It is considered that in the voltage and current dual-loop control, the bandwidth of the grid-connected current inner loop is usually designed to be wide ($K_{pwm}G_i(s) \gg Ls+r$). So, the expression (21) can be simplified as the practical feed-forward transfer function as follows:

$$G_{ff}(s)\approx -G_2(s)/G_l(s)=2U_{dc}/3U_q. \quad (22)$$

Combining the dc output current feed-forward control with the virtual inertia control, the closed-loop transfer function $TF_{ff}(s)$ between $\Delta u_{dc}(s)$ and $\Delta i_o(s)$ can be expressed as:

$$TF_{ff}(s)=\frac{\Delta u_{dc}(s)}{\Delta i_o(s)}=\frac{G_{vir}(s)G_v(s)G_c(s)G_l(s)}{1+G_v(s)G_c(s)G_l(s)}. \quad (23)$$

Fig. 8 shows the unit-step responses of $TF_{ff}(s)$ for various values of C_v when D_b = 5. The red solid points represent the positions where the step response curve reaches the 95% of the steady state value. Obviously, introducing the dc output

current feed-forward control and the virtual inertia control for the BGC, the unit-step responses of the dc bus voltage all smoothly decline to the steady state value, so the dynamic process of the dc bus voltage is improved.

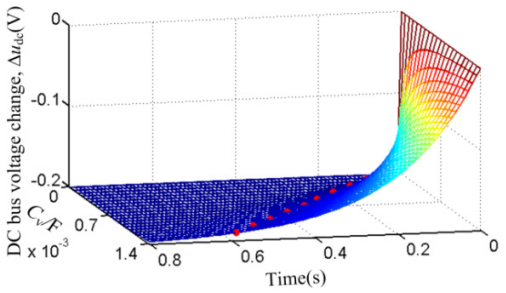

Fig. 8. Unit-step responses of $TF_{\mathrm{ff}}(s)$ for various values of C_{v} when $D_{\mathrm{b}} = 5$.

V. System Stability Analysis and Parameters Selection

Fig. 9 shows the zeros and dominant poles distribution diagram of $TF_{\mathrm{ff}}(s)$. The symbol "×" and "+" represent poles, the symbol "o" represents zero. It can be seen that two pairs of dipoles are in each sub-graph of Fig. 9. These dipoles are far away from the origin point so their impact on the control system can be neglected. In Fig. 9(a), a sole dominant pole moves with C_{v} changing. If $C_{\mathrm{v}} \geq 0$, the pole moves toward the imaginary axis with C_{v} increasing but it will not cross the imaginary axis. If $C_{\mathrm{v}} < 0$, the sole mobile pole is on the right side of the system so that the system is unstable. Therefore, for the stability of system, it is satisfactory enough when $C_{\mathrm{v}} \geq 0$. In Fig. 9(b), a sole dominant pole moves away from the imaginary axis with D_{b} increasing.

Seen from Fig. 9(a) and Fig. 9(b), there is only one dominant pole. Therefore, the dynamic performance of the high-order system can be estimated by the dynamic performance index of the first-order system. Using MATLAB, the sole dominant pole is calculated to be $-D_{\mathrm{b}}/(C_{\mathrm{v}}U_{\mathrm{n}})$ and the final value of the dynamic response is determined by D_{b}. Therefore, $TF_{\mathrm{ff}}(s)$ is approximately equal to:

$$TF_{\mathrm{ff}}(s) \approx -1/D_{\mathrm{b}}(1+\tau s) \tag{24}$$

where $\tau = C_{\mathrm{v}}U_{\mathrm{n}}/D_{\mathrm{b}}$. The time constant of the first-order system is $T = 3\tau = 3C_{\mathrm{v}}U_{\mathrm{n}}/D_{\mathrm{b}}$, which directly reflects the inertia of the first-order system. Assuming that D_{b} remains unchanged, T gets larger with C_{v} increasing, inertia of the DC-MG becomes larger, and the process of the dynamic response slows down, which makes it better to suppress the impact of the dc bus voltage caused by power fluctuation of the DC-MG. Conversely, when C_{v} is smaller, inertia of DC-MG becomes smaller and its ability to suppress the dc bus voltage fluctuation weakens. Therefore, the value of C_{v} should be reasonably set according to the above analysis and inertia requirement of the DC-MG.

In Fig. 9(c), when C_{v} is fixed, with C increasing, a dominant pole of the $TF_{\mathrm{ff}}(s)$ (surrounded by dotted green circle) is fixed. Its value is $-D_{\mathrm{b}}/C_{\mathrm{v}}U_{\mathrm{n}}$ which is related to C_{v} not C. But there are two changing poles when C changes. When C < 50mF, those poles are not the dominant ones. When C > 50mF, those poles are getting closer to the imaginary axis with C increasing and become the dominant poles apart from the fixed one. And the system damping decreases and is prone to cause the dc bus voltage oscillation when the power of the DC-MG suddenly changes. Those changing poles are called low frequency oscillatory modes [34].

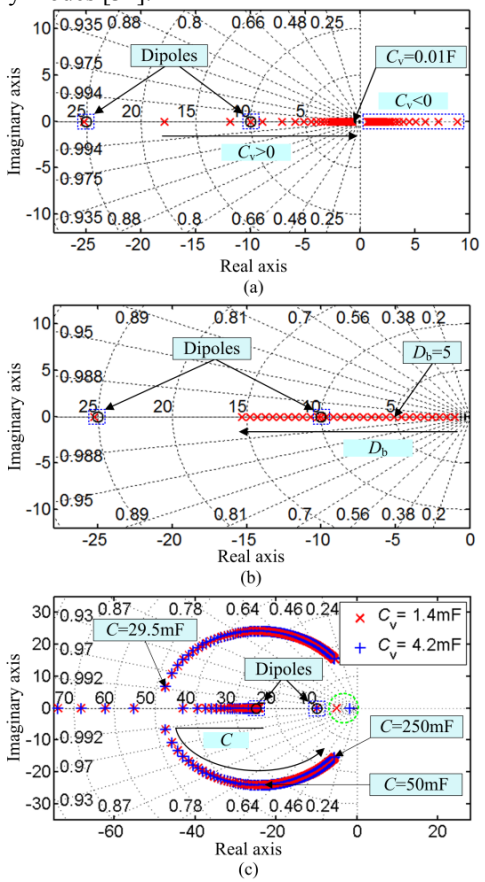

Fig. 9. Zeros and dominant poles distribution of $TF_{\mathrm{ff}}(s)$. (a) Arrow direction : C_{v} changes from 0mF to 10mF. (b) Arrow direction : D_{b} changes from 1 to 15. (c) Arrow direction : C changes from 0. 5mF to 250mF.

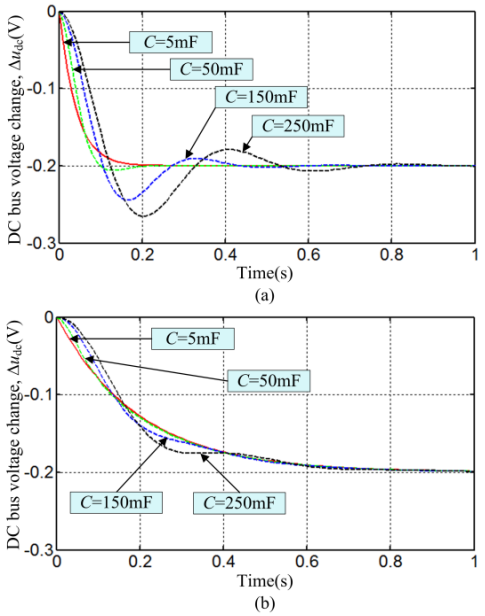

Fig. 10. Unit-step responses of $TF_{\mathrm{ff}}(s)$ for various values of C. (a) C_{v} = 0.28mF. (b) C_{v} = 1.4mF.

Fig. 10 shows the unit-step response of $TF_{\mathrm{ff}}(s)$ for various

values of C when C_v = 0.28mF or 1.4mF. In Fig. 10(a), C_v = 0.28mF, when C > 50mF, the dc bus voltage oscillation is rather obvious in the unit-step response of $TF_{ff}(s)$. In Fig. 10(b), C_v = 1.4mF, when C > 50mF, the dc bus voltage oscillation is less obvious in the unit-step response of $TF_{ff}(s)$, but the oscillation still exists. In Fig. 9(c), when C < 29.5mF, all the poles are located on the real axis and the $TF_{ff}(s)$ damping is above 1, thus, no low frequency oscillation will happen. Therefore, from the view of low frequency oscillatory modes, the maximum value of C has the corresponding limit.

In the VSM control, the small-signal closed-loop transfer function of the inverter output active power is a typical second-order system and it is described as follows:

$$\frac{\Delta P_e(s)}{\Delta P_{set}(s)} = \frac{\omega_{na}^2}{s^2 + 2\xi\omega_{na}s + \omega_{na}^2} \tag{25a}$$

$$\xi = \frac{D_p}{2}\sqrt{\frac{\omega_n}{JP_{max}}} \tag{25b}$$

$$\omega_{na} = \sqrt{\frac{P_{max}}{J\omega_n}} \tag{25c}$$

where P_{max} is the maximum output power of the inverter. From (25b), it can be seen that the damping factor ξ of the second-order system is proportional to D_p. However, it is known from (2) that D_p is inversely proportional to the droop coefficient of the P-ω droop. When an AC-MG operates in the islanded mode, the active power sharing between inverters is better if the droop coefficient of the P-ω control is larger. On the other hand, the larger damping factor ξ is，the better oscillation suppression effect is. Therefore, the damping factor ξ of the second-order system and the droop coefficient of the inverter are mutually constrained by D_p, making it difficult to set both the damping factor and the droop coefficient at their optimal values.

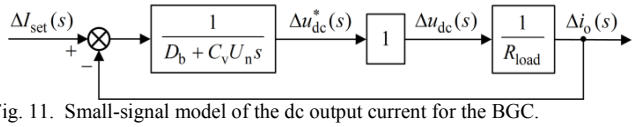

Fig. 11. Small-signal model of the dc output current for the BGC.

Different from the small-signal closed-loop transfer function of the VSM output active power, the small-signal closed-loop transfer function of the BGC output current is a first-order system, as shown in Fig. 11.

For simple analysis, the unity gain block represents the closed-loop gain of the dc bus voltage loop. For the BGC, the whole DC-MG is equivalent to a load and can be represented as R_{load}. From Fig. 11, the small-signal closed-loop transfer function of the dc output current for the BGC is obtained as:

$$\frac{\Delta i_o(s)}{\Delta I_{set}(s)} = \frac{1}{R_{load}C_vU_ns + R_{load}D_b + 1} \tag{26}$$

According to the analogy analysis in Section II, the dc output current of the BGC in the DC-MG is corresponding to the output active power of the inverter using VSM control in the AC-MG. From (26), it can be seen that the small-signal closed-loop transfer function of the dc output current for the BGC is the first-order inertia system so no oscillation exists in its dynamic response. Thus, the setting of D_b only needs to satisfy the requirement of the voltage-current droop coefficient.

Fig. 12 shows the unit-step responses of $TF_{ff}(s)$ for various values of D_b when C_v = 1.4mF. The magenta solid points represent the positions where the step response curve reaches the 95% of the steady state value. From Fig. 12 and (24), $1/D_b$ is proportional to the final value of the unit-step response of the system. Thus, the value of $1/D_b$ should satisfy the constraint condiction as follows:

$$\frac{1}{D_b} \le \frac{\Delta u_{dcmax}}{2i_{or}} \tag{27}$$

where i_{or} is the rated dc output current of the BGC. Δu_{dcmax} is the difference between the maximum and minimum dc bus voltages when the DC-MG is in grid-connected mode. When $1/D_b$ is larger, the stability range of the BGC with constant power loads is larger. In the grid-connected system, the larger $1/D_b$ means the better power sharing among each BGC. So $1/D_b = \Delta u_{dcmax}/(2i_{or})$, thus $D_b = 2i_{or}/\Delta u_{dcmax}$.

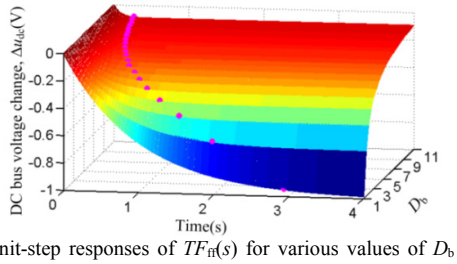

Fig. 12. Unit-step responses of $TF_{ff}(s)$ for various values of D_b when C_v = 1.4mF.

Noticeably, from Fig. 12, when C_v is determined, the change of D_b would influence the inertia. The smaller D_b means the larger system inertia, and vice versa. Therefore, D_b should be firstly selected before C_v.

The parameter design of voltage and current dual-loop control is decided by stability margin and system bandwidth. In order to attain better stability margin, satisfied anti-noise ability and quick dynamic response, the phase margin and bandwidth of the current inner-loop controller are 90° and 1 kHz, respectively. And those two parameters of the voltage outer-loop controller are 80° and 85Hz. According to the above performance indexes, the relevant controller parameters are shown in Table II. The switching frequency f_s of BGC is 10 kHz. The rated dc output current i_{or} of the BGC is 70A. The rated dc bus voltage U_n is 700V. In order to confine the bus voltage fluctuation within 2% of the rated value in the grid-connected mode, Δu_{dcmax} needs to be 28V, thus, $D_b = 2i_{or}/\Delta u_{dcmax}$ = 5. The fluctuation component of loads in DC-MG is often at millisecond level. Hence, in order to suppress the impact from this kind of fluctuation component, the time constant T sets to be 0.6s, then $C_v = TD_b/(3U_n)$ = 1.4mF. Considering the bidirectional energy flowing of the BGC, I_{set} is set to be 0. The function of the dc-side capacitor is to be as the buffer of energy exchange between AC and dc side of the BGC and to suppress the harmonic voltage on the dc side. And the filter inductor is used to restrict the grid-connected harmonic current. Based on engineering experience, C and L can be set at 5740μF and 1mH, respectively. The electrolytic capacitor bank C on the dc side is 5740μF, adopting the integrated

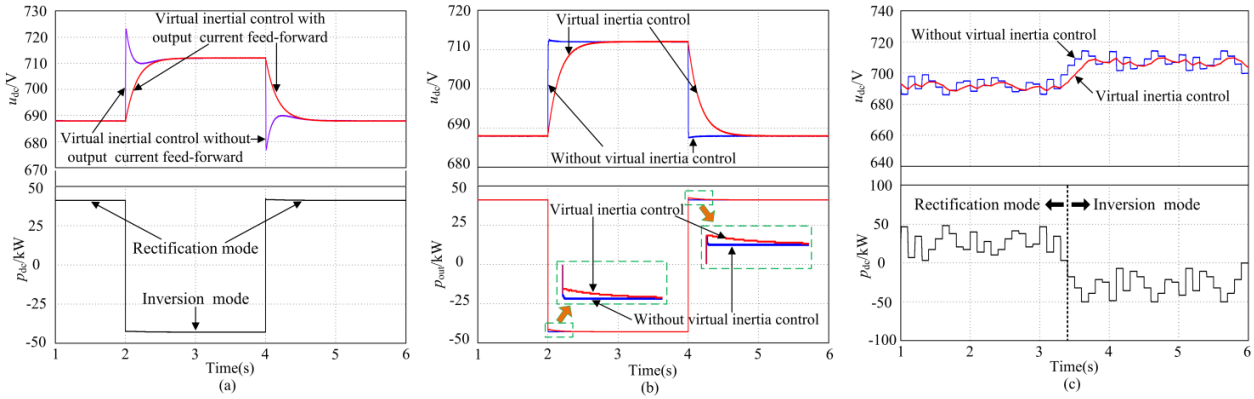

Fig. 13. Simulation results. (a) Virtual inertia control with or without dc output current feed-forward. (b) DC output current feed-forward control with or without virtual inertia control. (c) Simulation results when p_{dc} randomly fluctuates.

structure which has 14 parallel branches with 2 series electrolytic capacitors. Each capacitor is 820μF and its withstanding value is 450V.

VI. Simulations and Experiments

In order to verify the validity of the proposed control strategy, a DC-MG simulation platform is built in Psim according to Fig. 1. In this system, the maximum output power of the DGs is 50kW. The maximum power of the loads is 50kW. The rated dc bus voltage U_n is 700V. The system parameters of the BGC are listed in Table II.

TABLE II
SYSTEM PARAMETERS OF THE BGC

Parameters	Values	Parameters	Values
U_{dc_ref} (V)	700	k_{pv}	2
L (mH)	1	k_{iv}	100
C (μF)	5740	k_{pi}	0.1
C_v (mF)	1.4	k_{ii}	10
D_b	5	u_j (V)	380
I_{set}(A)	0	f_s(kHz)	10

Fig. 13(a) shows the simulation waveforms of the dc bus voltage u_{dc} when the power demand of the DC-MG p_{dc} suddenly changes. When t = 2s, p_{dc} suddenly declines from 41kW to −43kW. Adopting virtual inertia control without output current feed-forward, u_{dc} suddenly increases at first, and then drops down, and finally smoothly increases to the steady-state value. On the other hand, adopting virtual inertia control with output current feed-forward, u_{dc} smoothly increases to the steady state value and shows no conditions of sudden voltage ups and drops. When t = 4s, p_{dc} suddenly increases from −43kW to 41kW. Without the output current feed-forward, u_{dc} suddenly drops and then increases and finally smoothly declines to the steady state value. With the output current feed-forward, u_{dc} smoothly drops to the steady state value. Thus, the dynamic performance of the dc bus voltage can be improved by introducing the dc output current feed-forward control into the proposed BGC virtual inertia control.

Fig. 13(b) is the simulation results with or without (C_v = 0) the virtual inertia control when the BGC already adopts the dc output current feed-forward control, where p_{out} is the output power of the BGC. When p_{dc} abruptly changes, without the virtual inertia control, u_{dc} quickly reaches the steady state value. Using the virtual inertia control, u_{dc} arrives at the steady state value in a slower speed. When t = 2s, p_{dc} suddenly drops, without the virtual inertia control, the BGC transmits the spare power of DC-MG to the utility gird. When the virtual inertia control is employed, the BGC transmits less power toward the utility grid than that without the virtual inertia control. When t = 4s, p_{dc} suddenly increases. Using the virtual inertia control, the BGC can provide more power to the DC-MG than that without the virtual inertia control, immediately compensating the power shortage of the DC-MG. Therefore, no matter from the perspective of the dc bus voltage or the BGC output power, inertia of the DC-MG can be improved when the BGC uses the virtual inertia control.

Fig. 13(c) shows the simulation results when p_{dc} randomly and drastically fluctuates in a short-time period. Without the virtual inertia control, the bus voltage changes drastically and inertia is small. By introducing the virtual inertia control, the waveform of the dc bus voltage becomes smooth, and the voltage quality increases.

In order to further verify the theoretical analysis and the simulation results, the DC-MG experiment platform is built, as shown in Fig. 14. The BGC system parameters are identical with the simulation parameters in Table II.

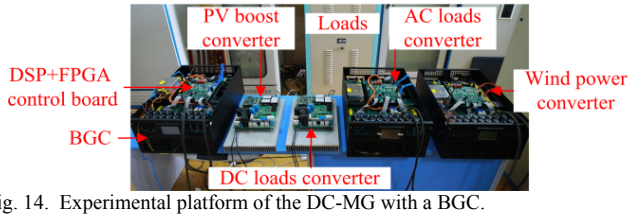

Fig. 14. Experimental platform of the DC-MG with a BGC.

Fig. 15 shows the experimental waveforms of the grid-connected current i_a and the dc bus voltage u_{dc} with different control strategies, when p_{dc} suddenly drops from 28kW to 4.7kW. In Fig. 15(a) u_{dc} soon reaches the steady state value after p_{dc} suddenly drops and system inertia is very small. In Fig. 15(b), at the moment when p_{dc} abruptly drops, u_{dc} experiences a sudden increase and then slowly arrives at the steady state value. The dynamic process of the dc bus voltage is not smooth. In Fig. 15(c) and Fig. 15(d), after the sudden drop of p_{dc}, u_{dc} slowly and smoothly reaches the steady state value, the

inertia of the DC-MG is enhanced. As a result, the larger C_v is, the stronger inertia of the DC-MG is.

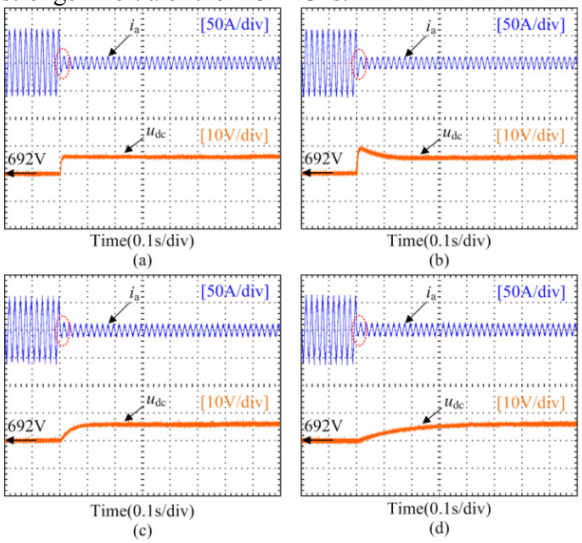

Fig. 15. Experimental results during sudden load step-down. (a) No virtual inertia control with dc output current feed-forward. (b) Virtual inertia control without dc output current feed-forward. (c) Virtual inertia control with dc output current feed-forward when C_v = 0.28mF. (d) Virtual inertia control with dc output current feed-forward when C_v = 1.4mF.

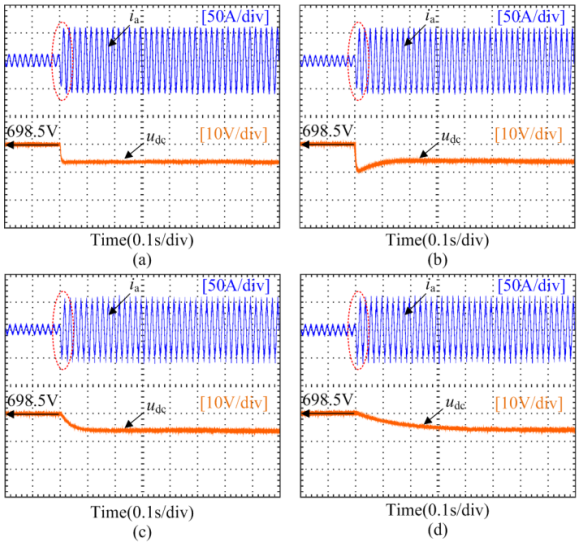

Fig. 16. Experimental results during sudden load step-up. (a) No virtual inertia control with dc output current feed-forward. (b) Virtual inertia control without dc output current feed-forward. (c) Virtual inertia control with dc output current feed-forward when C_v = 0.28mF. (d) Virtual inertia control with dc output current feed-forward when C_v = 1.4mF.

Fig. 16 shows the experimental waveforms of i_a and u_{dc} with different control strategies, when p_{dc} suddenly increases from 4.7kW to 28kW. From Fig. 16(a), u_{dc} quickly arrives at the steady state value after p_{dc} suddenly increases so the system inertia is very small. From Fig. 16(b), the dynamic process of u_{dc} is quite unsmooth which promptly decreases after p_{dc} suddenly increases, then returns and slowly increases to the steady state value. Fig. 16(c) and Fig. 16(d) show the experimental waveforms of the virtual inertia control with the dc output current feed-forward. It can be seen that u_{dc} slowly and smoothly falls to the steady state value after p_{dc} suddenly increases. Thus, the inertia of the DC-MG is strengthened and the larger C_v is, the longer the fall time and the stronger the inertia are.

Comparing the waveforms of the grid-connected current i_a of the BGC in Fig. 15 and Fig. 16, the inertia of the DC-MG is actually enhanced by increasing the energy exchange speed between the DC-MG and the utility grid. When p_{dc} decreases, i_a soon drops, thus the power quickly decreases. Similarly, when p_{dc} increases, i_a can increase quickly, thus the power immediately increases, restraining the dc bus voltage fluctuation and maintaining the stability of dc bus voltage.

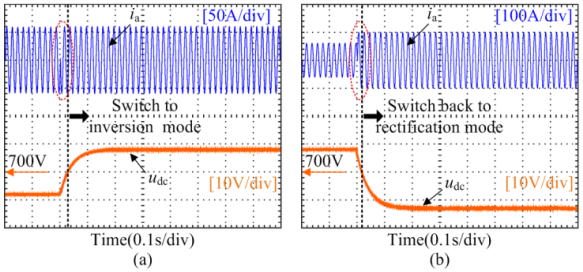

Fig. 17. Experimental results of the proposed control strategy during DC-MG operation mode changes when C_v = 0.28mF. (a) From rectification mode switch to inversion mode. (b) From inversion mode switch back to rectification mode.

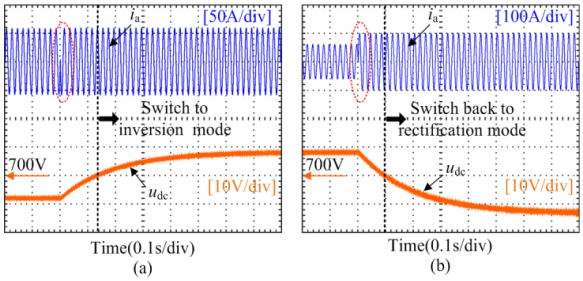

Fig. 18. Experimental results of the proposed control strategy during DC-MG operation mode changes when C_v = 1.4mF. (a) From rectification mode switch to inversion mode. (b) From inversion mode switch back to rectification mode.

Fig. 17 and Fig. 18 show the experimental results of the proposed control strategy under different operation modes changes when C_v is 0.28mF or 1.4mF. Fig. 17(a) and Fig. 18(a) are the waveforms of i_a and u_{dc} when the mode of BGC switches from the rectification mode to the inversion mode with p_{dc} suddenly dropping from 28kW to −28kW. Fig. 17(b) and Fig. 18(b) are the waveforms of i_a and u_{dc} when the mode of BGC switches from the inversion mode back to the rectification mode with p_{dc} suddenly dropping from −28kW to 45kW. It is obvious from Fig. 17 and Fig. 18 that when the power flow direction changes, the phase of the current wave suddenly changes 180° and the waveform of the voltage u_{dc} smoothly arrives at the steady state value so the proposed control strategy still can maintain the DC-MG inertia.

VII. CONCLUSION

Problems like the low inertia and the drastic dc bus voltage fluctuation jeopardizes the safe and steady operation of the DC-MG and reduces the system efficiency. In order to solve this problem, in this paper, a virtual inertia control strategy for DC-MG through the introduced BGC analogized with the VSM in AC-MG is proposed to enhance the inertia of the DC-MG, and to restrain the dc bus voltage fluctuation. The small-

signal model of the BGC system is built and the dynamic transfer function between the dc output current of the BGC and the dc bus voltage is deducted. It is also found that the dc output current of the BGC is equivalent to disturbance, which will have an impact on the dynamic process of the dc bus voltage. The dc output current feed-forward disturbance suppressing method for the BGC is introduced to smooth the dynamic response of the dc bus voltage. By analyzing the system stability, the proper control parameters of the BGC are selected. Moreover, the proposed control idea can also be extended to the control strategies of various kinds of converters in the DC-MG.

REFERENCES

[1] M. Hamzeh, A. Ghazanfari, Y. A.-R. I. Mohamed, and Y. Karimi, "Modeling and design of an oscillatory current-sharing control strategy in DC microgrids," *IEEE Trans. Ind. Electron*., vol. 62, no. 11, pp. 6647-6657, Nov. 2015.

[2] P. Huang, P. Liu, W. Xiao, and M. S. El Moursi, "A novel droop-based average voltage sharing control strategy for DC microgrids," *IEEE Trans. Smart Grid*, vol. 6, no. 3, pp. 1096-1106, May. 2015.

[3] X. Lu, K. Sun, J. M. Guerrero, J. C. Vasquez, and L. Huang, "State-of-charge balance using adaptive droop control for distributed energy storage systems in DC microgrid applications," *IEEE Trans. Ind. Electron*., vol. 61, no. 6, pp. 2804-2815, Jun. 2014.

[4] T. Wu, C. Chang, L. Lin, G. Yu, and Y. Chang, "DC-bus voltage control with a three-phase bidirectional inverter for DC distribution systems," *IEEE Trans. Power Electron*., vol. 28, no. 4, pp. 1890-1899, Apr. 2013.

[5] S. I. Ganesan, D. Pattabiraman, R. K. Govindarajan, M. Rajan, and C. Nagamani, "Control scheme for a bidirectional converter in a self-sustaining low-voltage DC nanogrid," *IEEE Trans. Ind. Electron*., vol. 62, no. 10, pp. 6317-6326, Oct. 2015.

[6] T. Dragičević, J. M. Guerrero, J. C. Vasquez, and D. Škrlec, "Supervisory control of an adaptive-droop regulated DC microgrid with battery management capability," *IEEE Trans. Power Electron*., vol. 29, no. 2, pp. 695-706, Feb. 2014.

[7] B. Liu, F. Zhuo, Y. Zhu, and H. Yi, "System operation and energy management of a renewable energy-based DC micro-grid for high penetration depth application," *IEEE Trans. Smart Grid*, vol. 6, no. 3, pp. 1147-1155, May. 2015.

[8] H. P. Beck, R. Hesse, "Virtual synchronous machine" in *9th International Conference on Electrical Power Quality and Utilisation*, Barcelona, Spain, 2007, pp. 1-6.

[9] Q.-C. Zhong and G. Weiss, "Synchronverters: Inverters that mimic synchronous generators," *IEEE Trans. Ind. Electron*., vol. 58, no. 4, pp. 1259-1267, Apr. 2011.

[10] Q.-C. Zhong, P.-L. Nguyen, Z. Ma, and W. Sheng, "Self-synchronized synchronverters: Inverters without a dedicated synchronization unit," *IEEE Trans. Power Electron*., vol. 29, no. 2, pp. 617-630, Feb. 2014.

[11] C. Li, J. Xu, and C. Zhao, "A coherency-based equivalence method for MMC inverters using virtual synchronous generator control," *IEEE Trans. Power Del*., vol. 31, no. 3, pp. 1369-1378, Jun. 2016.

[12] S. Wang, J. Hu, X. Yuan, and L. Sun, "On inertial dynamics of virtual-synchronous-controlled DFIG-based wind turbines," *IEEE Trans. Energy Convers*., vol. 30, no. 4, pp. 1691-1702, Dec. 2015.

[13] M. Guan, W. Pan, J. Zhang, Q. Hao, J. Cheng, and X. Zeng, "Synchronous generator emulation control strategy for voltage source converter (VSC) stations," *IEEE Trans. Power Syst*., vol. 30, no. 6, pp. 3093-3101, Nov. 2015.

[14] M. A. Torres L., L. A. C. Lopes, L. A. Morán T., and J. R. Espinoza C., "Self-tuning virtual synchronous machine: A control strategy for energy storage systems to support dynamic frequency control," *IEEE Trans. Energy Convers*., vol. 29, no. 4, pp. 833-840, Dec. 2014.

[15] J. Alipoor, Y. Miura, and T. Ise, "Power system stabilization using virtual synchronous generator with alternating moment of inertia," *IEEE J. Emerg. Sel. Topics Power Electron*., vol. 3, no. 2, pp. 451-458, Jun. 2015.

[16] T. Shintai, Y. Miura, and T. Ise, "Oscillation damping of a distributed generator using a virtual synchronous generator," *IEEE Trans. Power Del*., vol. 29, no. 2, pp. 668-676, Apr. 2014.

[17] M. Ashabani and Y. A.-R. I. Mohamed, "Integrating VSCs to weak grids by nonlinear power damping controller with self-synchronization capability," *IEEE Trans. Power Syst*., vol. 29, no. 2, pp. 805-814, Mar. 2014.

[18] H. Wu, X. Ruan, D. Yang, X. Chen, W. Zhao, Z. Lv, et al. "Small-signal modeling and parameters design for virtual synchronous generators," *IEEE Trans. Ind. Electron*., vol. 63, no. 7, pp. 4292-4303, Jul, 2016.

[19] J. Liu, Y. Miura, and T. Ise, "Comparison of dynamic characteristics between virtual synchronous generator and droop control in inverter-based distributed generators," *IEEE Trans. Power Electron*., vol. 31, no. 5, pp. 3600-3611, May. 2016.

[20] T. Dragicevié, X. Lu, J. C. Vasquez, and J. M. Guerrero, "DC microgrids—Part I: A review of control strategies and stabilization techniques," *IEEE Trans. Power Electron.*, vol. 31, no. 7, pp. 4876-4888, Jul. 2016.

[21] X. Lu, J. M. Guerrero, K. Sun, and J. C. Vasquez, "An improved droop control method for DC microgrids based on low bandwidth communication with DC bus voltage restoration and enhanced current sharing accuracy," *IEEE Trans. Power Electron*., vol. 29, no. 4, pp. 1800-1812, Apr. 2014.

[22] J. Schönberger, R. Duke, and S. Round, "DC-bus signaling: a distributed control strategy for a hybrid renewable nanogrid," *IEEE Trans. Ind. Electron.*, vol. 53, no. 5, pp. 1453-1460, Oct. 2006.

[23] S. Shin, H. Lee, Y. Kim, J. Lee, and C. Won, "Transient response improvement at startup of a three-phase AC/DC converter for a DC distribution system in commercial facilities," *IEEE Trans. Power Electron.*, vol. 29, no. 12, pp. 6742-6753, Dec. 2014.

[24] X. Cao, Q.-C Zhong, and W. Ming, "Ripple eliminator to smooth DC bus voltage and reduce the total capacitance required," *IEEE Trans. Ind. Electron.*, vol. 62, no. 4, pp. 2224-2235, Apr. 2015.

[25] Y. Levron, S. Canaday, and R. W. Erickson, "Bus voltage control with zero distortion and high bandwidth for single-phase solar inverters," *IEEE Trans. Power Electron*., vol. 31, no. 1, pp. 258-269, Jan. 2016.

[26] A. Hamad, H. Farag, and E. El-Saadany, "A novel multiagent control scheme for voltage regulation in DC distribution systems," *IEEE Trans. Sustain. Energy*, vol. 6, no. 2, pp. 534-545, Apr. 2015.

[27] B. Liu, F. Zhuo, and X. Bao, "Control method of the transient compensation process of a hybrid energy storage system based on battery and ultra-capacitor in micro-grid," in *Proc. IEEE ISIE Conf.* May. 2012, pp. 1325-1329.

[28] X. Zhu, J. Cai, Q. Yan, J. Chen, X. Wang, "Virtual inertia control of wind-battery-based islanded DC micro-grid," in *Proc. IET RPG Conf.* Oct. 2015, pp. 1-6.

[29] X. Lu, K. Sun, J. M. Guerrero, J. C. Vasquez, L. Huang, J. Wang, "Stability enhancement based on virtual impedance for DC microgrids with constant power loads," *IEEE Trans. Smart Grid*, vol. 6, no. 6, pp. 2770-2783, Nov. 2015.

[30] M. Wu and D. D.-C. Lu, "A novel stabilization method of *LC* input filter with constant power loads without load performance compromise in DC microgrids," *IEEE Trans. Ind. Electron*., vol. 62, no. 7, pp. 4552-4562, Jul. 2015.

[31] J. M. Guerrero, J. C. Vasquez, J. Matas, L. G. D. Vicuña, and M. Castilla, "Hierarchical control of droop-controlled AC and DC microgrids—A general approach toward standardization, " *IEEE Trans. Ind. Electron*., vol. 58, no. 1, pp. 158-172, Jan, 2011.

[32] C. Jin, P. Wang, J. Xiao, Y. Tang, and F. H. Choo, "Implementation of hierarchical control in DC microgrids," *IEEE Trans. Ind. Electron*., vol. 61, no. 8, pp. 4032-4042, Feb. 2014.

[33] S. Anand, B. G. Fernandes, and J. M. Guerrero, "Distributed control to ensure proportional load sharing and improve voltage regulation in low-voltage DC microgrids," *IEEE Trans. Power Electron*., vol. 28, no. 4, pp. 1900-1913, Apr. 2013.

[34] N. Pogaku, M. Prodanović, and T. C. Green, "Modeling, analysis and testing of autonomous operation of an inverter-based microgrid," *IEEE Trans. Power Electron.*, vol. 22, no. 2, pp. 613-625, Mar. 2007.

Wenhua Wu (S'16) was born in Hunan, China, 1991. He received the B.S. degree from the College of Electrical and Information Engineering, Hunan University, Changsha, China, in 2014. Currently, he has been working toward the Ph.D. degree in electrical engineering from Hunan University, Changsha, China.

His research interests include renewable energy generation systems, microgrid, power quality, and VSC-HVDC systems.

Yandong Chen (S'13-M'14) was born in Hunan, China, in 1979. He received the B.S. and M.S. degree in instrument science and technology from Hunan University, Changsha, China, in 2003 and 2006, respectively, and the Ph.D. degree in electrical engineering from Hunan University, Changsha, China, in 2014. He has been an Associate Professor in the College of Electrical and Information Engineering, Hunan University, Changsha.

His research interests include power electronics for microgrid, distributed generation, power quality, and energy storage. Dr. Chen is a recipient of the 2014 National Technological Invention Awards of China, and the 2014 WIPO-SIPO Award for Chinese Outstanding Patented Invention. He is a member of IEEE Power Electronics Society.

An Luo (SM'09) was born in Changsha, China, in 1957. He received the B.S. and M.S. degrees in industrial automation from Hunan University, Changsha, in 1982 and 1986, respectively, and the Ph.D. degree in fluid power transmission and control from Zhejiang University, Hangzhou, China, in 1993. Between 1996 and 2002, he was a Professor with Central South University. Since 2003, he has been a Professor in the College of Electrical and Information Engineering, Hunan University, where he also serves as the Chief of National Electric Power Conversion and Control Engineering Technology Research Center.

His research interests mainly include distributed generation, microgrid, and power quality. He was elected to the Chinese National Academy of Engineering (CNAE) in 2015, the highest honor for scientists and engineers and scientists in China. He has won the highly prestigious China National Science and Technology Awards three times (2014, 2010 and 2006).

Leming Zhou was born in Hunan, China, in 1989. He received the B.S. and Ph.D. degree in electrical engineering from Hunan University, Changsha, China, in 2011 and 2016, respectively. Currently, he has been working postdoctoral research in electrical engineering from Hunan University, Changsha, China.

His research interests include power electronics for microgrid, distributed generation, and power quality.

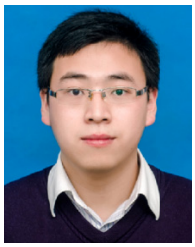

Xiaoping Zhou (S'16) was born in Jiangxi, China, 1990. He received the B.S. degree in electrical engineering from Hunan University, Changsha, China, in 2013. Currently, he has been working toward the Ph.D. degree in electrical engineering from Hunan University, Changsha, China.

His research interests include power electronics, distributed generation, microgrid, power quality and energy storage.

Ling Yang (S'16) was born in Liaoning, China, 1992. She received the B.S. degree from the College of Electrical and Information Engineering, Hunan University, Changsha, China, in 2014. Currently, she has been working toward the Ph.D. degree in electrical engineering from Hunan University, Changsha, China.

Her research interests include power electronics, and distributed power systems.

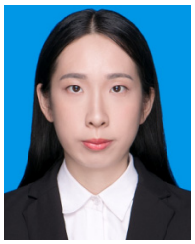

Yanting Dong was born in Guangdong, China, 1992. She received the B.S. degree from the College of Electrical and Information Engineering, Hunan University, Changsha, China, in 2014. Currently, she has been working toward the M.S. degree in electrical engineering from Hunan University, Changsha, China.

Her research interests include renewable energy generation systems and microgrid.

Josep M. Guerrero (S'01-M'04-SM'08-FM'15) received the B.S. degree in telecommunications engineering, the M.S. degree in electronics engineering, and the Ph.D. degree in power electronics from the Technical University of Catalonia, Barcelona, in 1997, 2000 and 2003, respectively. Since 2011, he has been a Full Professor with the Department of Energy Technology, Aalborg University, Denmark. From 2015 he is a distinguished guest Professor in Hunan University.

His research interests mainly include power electronics, distributed energy-storage, and microgrids. Prof. Guerrero is an Associate Editor for the IEEE TRANSACTIONS ON POWER ELECTRONICS, the IEEE TRANSACTIONS ON INDUSTRIAL ELECTRONICS, and the IEEE Industrial Electronics Magazine, and an Editor for the IEEE TRANSACTIONS on SMART GRID and IEEE TRANSACTIONS on ENERGY CONVERSION. In 2014, 2015, and 2016 he was awarded by Thomson Reuters as Highly Cited Researcher, and in 2015 he was elevated as IEEE Fellow for his contributions on distributed power systems and microgrids.